NAG5-11611

January 9, 2004

Nitric Acid Uptake on Subtropical Cirrus Cloud Particles

P.J. Popp*, R.S. Gao, T.P. Marcy*, D.W. Fahey*, P.K. Hudson*, T.L. Thompson
Aeronomy Laboratory, National Oceanic and Atmospheric Administration
Boulder, CO 80305
**Cooperative Institute for Research in Environmental Sciences, University of Colorado*

B. Kärcher
Institut für Physik der Atmosphäre, Deutsches Zentrum für Luft- and Raumfahrt
Oberpfaffenhofen, Germany

B.A. Ridley, A.J. Weinheimer, D.J. Knapp, D.D. Montzka
Atmospheric Chemistry Division, National Center for Atmospheric Research
Boulder, CO 80307

D. Baumgardner
Universidad Nacional Autonoma de Mexico, Centro de Ciencias de la Atmosfera
Ciudad Universitaria, 04510 Mexico DF, Mexico

T.J. Garrett
Department of Meteorology, University of Utah
Salt Lake City, UT 84112

E.M. Weinstock, J.B. Smith, D.S. Sayres, J.V. Pittman
Atmospheric Research Project, Harvard University
Cambridge, MA 02138

S. Dhaniyala
Division of Geology and Planetary Sciences, California Institute of Technology
Pasadena, CA 91125
Now at Department of Mechanical and Aeronautical Engineering, Clarkson University
Potsdam, NY 13699

T.P. Bui
NASA Ames Research Center
Moffett Field, CA 94035

M.J. Mahoney
Jet Propulsion Laboratory, California Institute of Technology
Pasadena, CA 91109

Abstract

The redistribution of HNO_3 via uptake and sedimentation by cirrus cloud particles is considered an important term in the upper tropospheric budget of reactive nitrogen. Numerous cirrus cloud encounters by the NASA WB-57F high-altitude research aircraft during CRYSTAL-FACE were accompanied by the observation of condensed-phase HNO_3 with the NOAA chemical ionization mass spectrometer. The instrument measures HNO_3 with two independent channels of detection connected to separate forward- and downward-facing inlets that allow a determination of the amount of HNO_3 condensed on ice particles. Subtropical cirrus clouds, as indicated by the presence of ice particles, were observed coincident with condensed-phase HNO_3 at temperatures of 197 K - 224 K and pressures of 122 hPa - 224 hPa. Maximum levels of condensed-phase HNO_3 approached the gas-phase equivalent of 0.8 ppbv. Ice particle surface coverages as high as $1.4 \cdot 10^{14}$ $\mathrm{molecules \cdot cm^{-2}}$ were observed. A dissociative Langmuir adsorption model, when using an empirically derived HNO_3 adsorption enthalpy of $-11.0\ \mathrm{kcal \cdot mol^{-1}}$, effectively describes the observed molecular coverages to within a factor of 5. The percentage of total HNO_3 in the condensed phase ranged from near zero to 100% in the observed cirrus clouds. With volume-weighted mean particle diameters up to 700 μm and particle fall velocities up to 10 $\mathrm{m \cdot s^{-1}}$, some observed clouds have significant potential to redistribute HNO_3 in the upper troposphere.

1. Introduction

Cirrus clouds are ubiquitous throughout the upper troposphere (UT) and can cover as much as 40% of the Earth's surface [*Liao et al.*, 1995, *Jin et al.*, 1996, *Wang et al.*, 1996, *Wylie and Menzel,* 1999]. Composed of ice crystals [*Lynch,* 2002], cirrus clouds are known to play a complex and significant role in the global radiation budget [*Liou*, 1986]. Cirrus clouds can be formed in situ in the UT [*Kärcher,* 2002], as a result of synoptic weather disturbances, or in the anvil outflow at the top of cumulonimbus clouds [*Sassen*, 2002]. Tropical cirrus clouds around the peak convective detrainment level are formed primarily via the latter mechanism, and can reach altitudes of up to 18 km when produced in deep convective systems. The broad lateral and vertical extent of anvil cirrus clouds produced in the tropics is expected to exert a greater influence on the Earth's climate system than midlatitude cirrus [*Heymsfield and McFarquhar*, 2002]. Due to the high altitudes and often-remote locations of tropical cirrus, however, comprehensive in situ measurements of these clouds have been limited.

Model simulations by *Lawrence and Crutzen* [1998] suggest that the uptake and gravitational redistribution of nitric acid (HNO_3) by cirrus cloud particles may represent a significant sink of HNO_3 in the UT. Nitric acid serves as a primary reservoir species for nitrogen oxides (NO_x) [*Neuman et al.*, 2001], which are directly involved in the photochemical production of tropospheric ozone [*Jaeglé et al.*, 1998]. Model studies of cirrus-processed air have demonstrated that the sedimentary removal of HNO_3 from the UT can effect strong local reductions in NO_x, with the consequence of significant reductions in the net ozone production rate [*Meier and Hendricks*, 2002]. Since ozone is known to be an effective greenhouse gas in the troposphere [*Albritton et al.*, 2001], particularly near the tropopause [*Lacis et al.*, 1990], understanding the uptake and redistribution of HNO_3 by cirrus cloud particles may be important in assessing the contribution of cirrus clouds to the radiative forcing of climate change.

A number of laboratory studies have investigated the uptake of HNO_3 on ice surfaces at temperatures typical of the UT. Experiments performed by *Zondlo et al.* [1997] on vapor-deposited ice films at 211 K resulted in observed HNO_3 surface coverages of $1.5 \cdot 10^{15}$ molecules·cm^{-2}. A series of similar experiments reported by *Hudson et al.* [2002] at an HNO_3 pressure ($P(HNO_3)$) of $1.1 \cdot 10^{-6}$ hPa indicated a negative temperature dependence to the observed uptake, with coverages of $1.1 \cdot 10^{14}$ to $5.9 \cdot 10^{13}$ molecules·cm^{-2} over a temperature range of 214-220 K. Uptake studies performed on ice films by *Abbatt* [1997] yielded coverages of up to $2.9 \cdot 10^{14}$ molecules·cm^{-2} at temperatures as low as 208 K, with no apparent dependency on $P(HNO_3)$ values over the range $1.7 \cdot 10^{-7}$ to $4.1 \cdot 10^{-6}$ hPa. *Hynes et al.* [2002] reported comparable coverages using a similar technique, although they observed coverages increasing by factor of 2 over a nearly 10-fold increase in $P(HNO_3)$, from $5.0 \cdot 10^{-7}$ - $3.0 \cdot 10^{-6}$ hPa. A laboratory study of HNO_3 uptake on nebulized half-micron diameter ice particles at 230 K yielded coverages similar to those observed on the ice films ($1.2 \cdot 10^{14}$ molecules·cm^{-2}), although these experiments were performed at the relatively high $P(HNO_3)$ of $7 \cdot 10^{-6}$ hPa [*Arora et al.*, 1999]. There has not yet been an extensive laboratory study of HNO_3 uptake on ice surfaces performed at $P(HNO_3)$ values typical of the UT ($< 2.0 \cdot 10^{-7}$ hPa).

Prior field studies of HNO_3 uptake on cirrus cloud particles have been made at mid and high latitudes. Measurements of total reactive nitrogen ($NO_y = NO + NO_2 + 2N_2O_5 + HNO_3 + \ldots$) in a mountain wave cloud over the continental United States reported by *Weinheimer et al.* [1998] indicated that levels of condensed NO_y in the cloud approached 20% of total NO_y. Surface coverages on the wave cloud ice particles were calculated to be as high as $2.5 \cdot 10^{13}$ molecules·cm^{-2} [*Hudson et al.*, 2002]. Measurements of condensed-phase NO_y in cirrus layers in the Arctic UT by *Kondo et al.* [2003] yielded HNO_3 coverages as high as $1.6 \cdot 10^{14}$ molecules·cm^{-2} at temperatures of approximately 200 K, with coverages decreasing at warmer temperatures. *Meilinger et al.* [1999] conducted similar measurements in Arctic cirrus clouds at 196 K and reported coverages of only $1 \cdot 10^{13}$ molecules·cm^{-2}. An extensive dataset of measurements made at midlatitudes revealed median levels of condensed NO_y (assumed to be HNO_3) in the northern hemisphere of $3.6 \cdot 10^{12}$ molecules·cm^{-2} to be greater than twice that observed in the southern hemisphere [*Ziereis et al.*, 2003]

We report here an extensive dataset of in situ measurements, including gas- and condensed-phase HNO_3 and ice particle surface area density (SAD), obtained in subtropical in situ and anvil cirrus clouds. These measurements were conducted onboard the NASA WB-57F high-altitude research aircraft as part of the Cirrus Regional Study of Tropical Anvils and Cirrus Layers Florida Area Cirrus Experiment (CRYSTAL-FACE) mission. The data are used here to assess the uptake of HNO_3 by subtropical cirrus cloud particles and explore the partitioning of HNO_3 between the gas and ice particle phases in cirrus clouds.

2. Instrumentation

This study utilizes data from a number of in situ instruments onboard the NASA WB-57F aircraft. Gas-phase and condensed-phase HNO_3 measurements made by chemical ionization mass spectrometry are described in more detail below. Particle size distribution and number density measurements made by the Cloud, Aerosol and Precipitation Spectrometer (CAPS) were used to derive SAD and volume-weighted mean diameter (VMD) for ice particles in the size range between 0.35-1550 μm [*Baumgardner et al.*, 2001]. Note that all particle sizes cited herein refer to particle diameter, and not radius. A second, independent measurement of SAD was provided by the Cloud Integrating Nephelometer (CIN) [*Gerber et al.*, 2000]. Ice water content (IWC) and water (H_2O) vapor were measured by the Harvard University Lyman-α hygrometer [*Weinstock et al.*, 1994, *Weinstock et al.*, 2003]. Nitric oxide (NO) and total reactive nitrogen (NO_y) were measured by catalytic reduction and chemiluminescence [*Weinheimer et al.*, 2003]. Ambient temperature and pressure, and WB-57F true air speed were measured by the Meteorological Measurement System (MMS) [*Scott et al.*, 1990]. The precision and accuracy of these measurements are summarized in Table 1.

Tropopause height was measured by the microwave temperature profiler (MTP) [*Denning et al.,* 1989].

2.1. HNO_3 Measurements

HNO_3 was measured using the NOAA chemical ionization mass spectrometer (CIMS) located in the third pallet position of the NASA WB-57F aircraft. This instrument measures HNO_3 with an accuracy of ±20% and precision of 30 pptv (1σ, 10-s averages), and has been described in detail elsewhere [*Neuman et al.*, 2000]. Prior to CRYSTAL-FACE, the NOAA CIMS was modified by the addition of a second independent channel for the measurement of HNO_3 and the relocation of the original sample inlet on the CIMS inlet pylon (Fig. 1). The two CIMS channels are designed to provide identical measurements of gas-phase HNO_3. Due to differences in the particle sampling efficiencies of the two inlets, however, the two channels have different sensitivity to condensed-phase HNO_3. When sampling in cirrus clouds, the forward-facing front inlet samples both gas-phase HNO_3 and any HNO_3 condensed on the cirrus particles. The downward-facing bottom inlet samples primarily gas-phase HNO_3 because the plane of the sampling orifice is parallel to the direction of flow over the inlet, which is set by the flow straightener. Semi-empirical calculations indicate that approximately 50% of 0.1 μm particles and greater than 90% of 1 μm and larger particles are inertially stripped from the air sampled by the bottom inlet [*Vincent et al.*, 1986]. Calculations further suggest that ice particles greater than 10 μm in diameter (typical of cirrus clouds observed during CRYSTAL-FACE) are almost entirely removed from the sampled air. Thus, for most of the cirrus clouds sampled, the HNO_3 from the bottom inlet is taken to be a measure of the gas-phase HNO_3 abundance.

The conclusion that ice particles greater than approximately 1 μm are inertially separated from air sampled by the bottom inlet is further supported by measurements made in the contrail of the WB-57F during CRYSTAL-FACE. The contrail contained ice particles with high number densities (100-200 cm^{-3}) and volume-weighted mean diameters on the order of 2 μm [*Gao et al.*, 2003]. HNO_3 was present in the contrail because of mixing between the exhaust gases and ambient air containing approximately 0.4 ppbv HNO_3. Measurements in the contrail as soon as 4 minutes after formation indicated a difference between the front and bottom CIMS channels. The minimum signal from the bottom channel was near zero inside the contrail. This low HNO_3 signal is consistent with the removal of gas-phase HNO_3 by uptake onto the 2-μm ice particles in the contrail, and the inertial stripping of these particles from the bottom inlet sample flow. As expected, a simultaneous increase in HNO_3 above ambient values occurred in the front CIMS channel, which does not discriminate against 2 μm particles. If the bottom CIMS inlet sampled 2 μm particles with any significant efficiency, HNO_3 observed in the bottom channel during the contrail intercept would not be significantly lower than the ambient values immediately outside the contrail.

The front CIMS inlet samples subisokinetically, meaning the sample air velocity inside the inlet (U) is less than the WB-57F true air speed (U_0) of 140-200 $m \cdot s^{-1}$ at sampling altitudes. As a result, cirrus cloud particle number densities in the sampled air stream are inertially enhanced relative to those in the ambient air. A computational fluid dynamics program (Fluent Inc., New Hampshire) was used to estimate particle enhancement factors (EF) in the front inlet by simulating the flow field and particle trajectories around a two-dimensional horizontal cross section of the CIMS pylon and inlet structure (Fig. 1). The value of EF is near unity for small particles (< 0.1 μm) and increases with particle size, as found for similar configurations [*Northway et al.*, 2002]. For particles larger than approximately 10 μm in diameter, typical of cirrus cloud ice particles sampled during CRYSTAL-FACE, EF for the front inlet approaches the maximum value of U_0/U. Since both CIMS channels sample at a constant mass flow of 1.85 standard liters per minute (slpm), U, and therefore, EF, are dependent upon the ambient temperature and pressure. Under typical WB-57F sampling conditions during CRYSTAL-FACE (temperature = 213 K, pressure = 170 hPa, $U_0 = 200\ m \cdot s^{-1}$), EF has a maximum value of approximately 16.

Cirrus cloud particles entering the front CIMS inlet travel through a 20 cm length of Teflon™ tubing (6.4 mm outside diameter, 4.0 mm inside diameter) upstream of the CIMS flow control valve and flow tube (Fig. 1). The use of Teflon™ sample lines ensures that HNO_3 will not readily absorb on the inlet surfaces [*Neuman et al.*, 1999]. This tubing, which is heated to 48° C in flight, has two bends to help ensure that large particles entering the inlet will impact on the tubing walls and subsequently evaporate prior to reaching the flow control valve. Particles with diameters greater than approximately 20 μm have large enough stopping distances at the freestream velocity that they impact at the first bend. Some particles that do not fully evaporate will impact in the body of the flow control valve or the flow tube entrance. HNO_3 condensed on the particle surfaces is liberated to the gas phase early in the evaporation process and measured as a gas-phase equivalent volume mixing ratio. The HNO_3 mixing ratio measured by the front CIMS channel, therefore, represents the sum of the gas- and the condensed-phase values, with the condensed-phase component enhanced by the value of *EF*.

3. Observations

Condensed-phase HNO_3 was observed coincident with cirrus cloud observations on 4 WB-57F science flights conducted as part of CRYSTAL-FACE. These flights originated and terminated at the United States Naval Air Facility, Key West (24.6° N, 81.7° W) in Florida on July 11, 13, 19 and 21, 2002. Time series data of HNO_3 mixing ratios observed from the front and bottom CIMS channels ($HNO_3|_{front}$ and $HNO_3|_{gas}$, respectively), as well as particle SAD, IWC (represented as a gas-phase equivalent volume mixing ratio) and meteorological parameters are shown for July 11, 13, 19 and 21 in Figs. 2-5, respectively. The presence of cirrus cloud particles is indicated by increases in SAD and IWC above background values. The presence of condensed-phase HNO_3 in a flight segment is indicated by $HNO_3|_{front}$ values that are significantly greater than

$HNO_3|_{gas}$ values. Flight segments identified by purple bars in panel (b) for July 13 (Fig. 3) and July 19 (Fig. 4) represent the observation of contrail cirrus clouds. As stated previously, these clouds are characterized by having high particle number densities with volume-weighted mean diameters typically much lower than cirrus clouds formed by natural processes. Due to the uncertainties in the SAD measurements in the contrail-formed cirrus clouds and in the value of *EF* for particles in this size range, these clouds are not considered in the data analysis presented here.

Cirrus clouds were observed from the WB-57F at pressures between 122 hPa and 224 hPa during the flights of July 11, 13, 19 and 21, corresponding to pressure altitudes between 11 km and 15 km (Figs. 2-5). These clouds were observed at temperatures between 197 K and 224 K. Figures 2-5 show the strong temporal correlation of ($HNO_3|_{front}$ - $HNO_3|_{gas}$) with both SAD and IWC in cirrus clouds, with $HNO_3|_{gas}$ approaching zero during a number of cirrus events. Outside of clouds, measured values of $HNO_3|_{front}$ and $HNO_3|_{gas}$ generally agree well (with an overall correlation coefficient, r, of 0.92). However, some periods in Figs. 2-5 show offsets between the two channels that are best explained as changes in the inlet line surfaces during the flight. Figure 4 also indicates elevated values of relative humidity (with respect to ice) during a number of cirrus cloud encounters, as described by *Gao et al.* [2003].

Condensed-phase HNO_3, proportional to the difference between the values of $HNO_3|_{front}$ and $HNO_3|_{gas}$, was observed primarily at SADs greater than 200 $\mu m^2 \cdot cm^{-3}$ during CRYSTAL-FACE (Fig. 6). Note that for the values of ($HNO_3|_{front}$ -$HNO_3|_{gas}$) shown in Fig. 6, $HNO_3|_{front}$ is not corrected for particle oversampling. Values of ($HNO_3|_{front}$ -$HNO_3|_{gas}$) at SADs less than 200 $\mu m^2 \cdot cm^{-3}$ are near the detection limit and highly variable due to CIMS instrument noise. In the analyses presented here, observations at SADs greater than 200 $\mu m^2 \cdot cm^{-3}$ are selected to represent measurements made in cirrus clouds (shown by the dashed line in Fig. 6).

3.1. Quantifying Condensed-Phase HNO_3

As stated previously, $HNO_3|_{front}$ represents the sum of gas-phase and condensed-phase HNO_3, with the condensed-phase component enhanced by the value of *EF*. The amount of HNO_3 condensed on cirrus cloud particles ($HNO_3|_{con}$) can therefore be calculated according to equation (1),

$$HNO_3|_{con} = \frac{HNO_3|_{front} - HNO_3|_{gas}}{EF} \qquad (1)$$

where $HNO_3|_{con}$ is reported as a gas-phase equivalent volume mixing ratio with a precision of 3 pptv (1σ, 10-s averages). The use of equation (1) in calculating $HNO_3|_{con}$ is illustrated in Fig. 7 for a cirrus cloud encounter by the WB-57F on July 13, 2002. Increases in SAD and IWC during this cloud event are accompanied by an increase in $HNO_3|_{front}$ above the gas-phase value of approximately 0.5 ppbv (Fig. 7a,d,e). Accounting for the particle enhancement factor of approximately 13.7 using equation (1), maximum values of $HNO_3|_{con}$ during this cloud event approached 0.1 ppbv (Fig. 7b,c). It should be noted here that calculated values of $HNO_3|_{con}$ in cirrus clouds are not always consistent with the observed decreases in $HNO_3|_{gas}$ that result from HNO_3 uptake. Quantitative agreement between $HNO_3|_{con}$ and deficits in $HNO_3|_{gas}$ can only occur if the cloud particles are sampled in the same air mass in which uptake occurred. Due to gravitational settling, however, cirrus particles may sediment into air masses that may be more or less depleted in gas-phase HNO_3 at the time of sampling.

3.2. Cirrus Cloud Particle Measurements

Cirrus cloud particle SAD was derived from measurements provided by both the CAPS and CIN instruments onboard the WB-57F during CRYSTAL-FACE. SAD was derived from the CAPS data by integrating particle size distribution and number density measurements, while bulk measurements of cloud extinction coefficient at 635 nm were used to derive SAD from the CIN data. A comparison between the CIN- and CAPS-derived SADs indicates good agreement between the two instruments for the flights on

July 11, 19 and 21, with SADs derived from the CIN measurements ranging from 23-39% higher than the CAPS-derived values on those 3 flight days (Fig. 8). On July 13, the CIN measurements were 54% higher than the CAPS values, which may be attributable to the sampling of optically thin subvisual cirrus clouds near the tropopause on that day. Cloud extinction in these subvisual cirrus is close to the sensitivity threshold of the CIN. The observed differences are nonetheless within the combined uncertainties of the two instruments on all 4 flight days. The analyses presented here make use of SADs derived from the CAPS measurements. Due to the fact that the SADs derived from the CIN measurements are 23-54% higher than the CAPS values, the SADs utilized here can be considered lower limits.

As stated previously, the value of *EF* used in calculating $HNO_3|_{con}$ approaches a maximum value of U_0/U (the ratio of the WB-57F true air speed to the air velocity in the sample inlet) at particle sizes greater than approximately 10 μm. SADs calculated from the CAPS measurements on the 4 flight days considered here (in cirrus clouds with total SADs greater than 200 $\mu m^2 \cdot cm^{-3}$) indicate that 92±9% of the surface area resides on particles larger than 10 μm in diameter. Use of the maximum value of *EF* in calculating $HNO_3|_{con}$ via equation (1), therefore, is expected to introduce no more than 10% uncertainty into the value of $HNO_3|_{con}$.

The VMD of cirrus cloud particles observed during CRYSTAL-FACE ranged from approximately 3 μm up to 700 μm, with most clouds having VMDs greater than 20 μm (Fig. 9a). The largest particles (> 500 μm) were observed primarily in clouds with SADs greater than 10^4 $\mu m^2 \cdot cm^{-3}$. As expected, IWC shows a strong correlation with SAD (Fig. 9b). IWCs as high as 1000 ppmv were observed during some cloud events (Fig. 9b). The highest values of VMD and IWC were observed from the WB-57F primarily at temperatures between 205 K and 215 K during the flights shown in Fig. 9.

4. Discussion

4.1. HNO_3 Uptake on Cirrus Cloud Particles

The coincident observation of cirrus clouds and condensed-phase HNO_3 during CRYSTAL-FACE is assumed here to result from the uptake of HNO_3 on the surface of cirrus cloud particles. Laboratory studies indicate that the low solubility of HNO_3 in ice will not allow a significant fraction of $HNO_3|_{con}$ to reside in the bulk of the cirrus particles [*Sommerfeld et al*, 1998, *Hanson and Ravishankara*, 1991]. Furthermore, *Dominé and Thibert* [1996] have suggested that the high diffusivity of HNO_3 in ice is such that HNO_3 trapped in the bulk ice during particle formation will migrate to the particle surface. We note, however, that the measurements presented here cannot distinguish between surface uptake and HNO_3 that may be condensed in the bulk of the particles. HNO_3 uptake on cirrus cloud particles can be represented in terms of molecular coverage, given by the ratio of $HNO_3|_{con}$ to SAD in units of molecules·cm^{-2}. HNO_3 surface coverages observed during CRYSTAL-FACE are shown as a function of temperature in Fig. 10, with symbols colored according to $P(HNO_3)$ (see legend). Data shown by triangles at temperatures less than 200 K in Fig.10 represent observations under conditions in which nitric acid trihydrate (NAT) is stable, as predicted by ambient temperature and the ratio of $HNO_3|_{gas}$ to H_2O vapor [*Hanson and Mauersberger,* 1988, *Gao et al.,* 2003]. It has been proposed that, under conditions in which NAT is stable, HNO_3 forms NAT clusters or layers on the particle surface which interfere with the condensation of H_2O molecules on the particle surface, and thereby increase the relative humidity with respect to ice in the cirrus cloud [*Gao et al.*, 2003].

The mean HNO_3 coverage observed during CRYSTAL-FACE was $1.9 \cdot 10^{13}$ molecules·cm^{-2}, with maximum coverages reaching $1.4 \cdot 10^{14}$ molecules·cm^{-2} during a few cirrus cloud events (Fig. 10). While the greatest coverages were observed at temperatures between 205 K and 210 K, mean coverages binned according to temperature show no temperature dependence above 200 K (black symbols in Fig. 10). The average value for measurements between 195 K and 200 K is approximately a factor of 3 greater than values above 200 K. Generally higher HNO_3 coverages at lower temperatures have been observed in field measurements reported by both *Kondo et al.* [2003] and *Ziereis et al.* [2003]. HNO_3 coverages show a minimal dependence on $P(HNO_3)$, with the lowest coverages occurring at $P(HNO_3)$ values below $2.5 \cdot 10^{-8}$ hPa (Fig. 10). A number of laboratory studies have also reported increased HNO_3 coverages with increasing $P(HNO_3)$, albeit at $P(HNO_3)$ values substantially higher than those presented here ($5.0 \cdot 10^{-7}$ - $3.0 \cdot 10^{-6}$ hPa) [*Hudson et al.*, 2002, *Hynes et al.*, 2002]. These results highlight the need for a comprehensive laboratory study of HNO_3 uptake on ice surfaces at $P(HNO_3)$ values below $2.0 \cdot 10^{-7}$ hPa that are typical of the subtropical UT.

The coverage of HNO_3 on ice, in general, can be modeled or predicted using the kinetics or thermodynamics of the uptake process [*Gao et al.*, 2003, *Hudson et al.*, 2002]. Using laboratory measurements and a semi-empirical equilibrium surface coverage model, *Hudson et al.* [2002] have predicted HNO_3 coverage on ice surfaces as a function of temperature and $P(HNO_3)$. This multilayer Frenkel-Halsey-Hill (FHH) model was fitted to equilibrium HNO_3 coverages observed on vapor-deposited ice films at temperatures between 213 K and 219 K with a $P(HNO_3)$ of $1.1 \cdot 10^{-6}$ hPa. HNO_3 surface coverages predicted by the FHH model are shown as a function of temperature in Fig. 11a, together with the HNO_3 coverages observed in cirrus clouds during CRYSTAL-FACE. The isobaric lines representing the modeled coverages are colored on the same scale as the observed coverages according to the values of $P(HNO_3)$ input to the model. Fig 11a indicates better agreement between the modeled and observed HNO_3 coverages at temperatures higher than approximately 205 K, while at lower temperatures the modeled coverages increase to values far greater than those observed at comparable temperatures and $P(HNO_3)$ values. The high model coverages below 205 K may result from the fact that the model was fitted to laboratory data at temperatures above 213 K, and the coverages presented here, therefore, are extrapolated to lower temperatures where the uncertainty in the model increases.

A number of studies have described the uptake of HNO_3 on ice surfaces using a

Langmuir surface chemistry model [*Tabazdeh et al.*, 1999, *Hynes et al.*, 2002, *Meier et al.*, 2002]. The Langmuir isotherm predicts the fractional HNO_3 surface coverage (θ) according to equation 2,

$$\theta = \frac{K_{eq}^{1/2} \cdot P(\mathrm{HNO_3})^{1/2}}{1 + K_{eq}^{1/2} \cdot P(\mathrm{HNO_3})^{1/2}} \qquad (2)$$

where K_{eq} represents the equilibrium adsorption constant, given by the ratio of the rates of adsorption and desorption (k_a/k_d) [*Laidler and Meiser*, 1982]. The value of θ is unity when the HNO_3 surface coverage reaches a complete monolayer ($1.0 \cdot 10^{15}$ molecules·cm^{-2}). We note that the surface density of HNO_3 molecules when forming a complete monolayer is somewhat uncertain, and the density of $1.0 \cdot 10^{15}$ molecules·cm^{-2} stated here should be considered an upper limit [*Hudson et al.*, 2002]. If the HNO_3 surface density is lower than $1.0 \cdot 10^{15}$ molecules·cm^{-2} for a complete monolayer, the resulting fractional surface coverages will be higher than those stated here. Application of the dissociative form of the Langmuir isotherm is supported here by spectroscopic studies of HNO_3 uptake on thin ice films at 211 K, which indicate, by the presence of H_3O^+ and NO_3^- ions on the ice surface, that HNO_3 dissociates upon adsorption [*Zondlo et al.*, 1997]. The temperature-dependent equilibrium adsorption constant in equation (2) can be calculated according to equation (3) [*Adamson and Gast*, 1997],

$$K_{eq} = \frac{100 \cdot \mathrm{N_A} \cdot \sigma_0 \cdot \tau_0}{(2\pi \cdot \mathrm{M} \cdot \mathrm{R} \cdot \mathrm{T})^{1/2}} \, e^{\left(\frac{-\Delta H_{ads}}{c \cdot \mathrm{R} \cdot \mathrm{T}}\right)} \ \mathrm{hPa}^{-1} \qquad (3)$$

where N_A is Avogadro's number ($6.02 \cdot 10^{23}$ mol^{-1}), σ_0 is the area of one adsorption site (10^{-19} m^2), τ_0 is the time constant for adsorbate oscillation perpendicular to the surface (10^{-13} s), M is the molecular weight of HNO_3 (0.063 kg·mol^{-1}), R is the ideal gas constant (8.314 J·mol^{-1}·K^{-1}), T is temperature (in K), c is a unit conversion factor ($2.39 \cdot 10^{-4}$ kcal·J^{-1}) and ΔH_{ads} is the adsorption enthalpy of HNO_3 on ice (in kcal·mol^{-1}).

Using equations (2) and (3), a Langmuir isotherm was fitted to the CRYSTAL-FACE observations of fractional surface coverage and $P(HNO_3)$ (Fig. 12). Using the median temperature of 208 K for the observations shown in Fig. 9, the best fit to the experimental data was achieved with a ΔH_{ads} of -11.0 kcal·mol^{-1}, or 46.0 kJ·mol^{-1} (red line in Fig. 12). Note that the data are largely bound by ΔH_{ads} values of -10.0 kcal·mol^{-1} and -12.0 kcal·mol^{-1}. Also shown in Fig. 12 are Langmuir isotherms at the same temperature for ΔH_{ads} values of -14.2 kcal·mol^{-1} and -12.9 kcal·mol^{-1} reported by *Tabazadeh et al.* [1998] and *Hynes et al.*, [2002], respectively. Fractional coverages predicted using these previously published values of ΔH_{ads} far exceed the coverages observed during CRYSTAL-FACE, indicating these adsorption enthalpies are too high to accurately describe the observations presented here. *Bartels-Rausch et al.* [2002], using a chromatographic technique, have recently reported a ΔH_{ads} for HNO_3 uptake on ice of -10.5 kcal·mol^{-1} that is in good agreement with the value of -11.0 kcal·mol^{-1} presented here. We caution that the effective ΔH_{ads} reported here is empirically derived from observations in a dynamic system which may or may not be in steady state, and this value, therefore, cannot be considered a fundamental thermodynamic parameter. Nonetheless, the Langmuir formalism, using a ΔH_{ads} of -11.0 kcal·mol^{-1}, effectively describes the CRYSTAL-FACE observations of HNO_3 uptake on cirrus cloud particles to within a factor of 5 (Fig. 12). It should be noted that the data shown in Fig. 12 span a temperature range form 197 K to 218 K, and that the Langmuir isotherms were fitted at the median temperature of 208 K. Use of a single temperature in fitting the isotherms is supported by the results of *Hynes et al.* [2002], who reported a variation of less than 2% between values of ΔH_{ads} derived from laboratory measurements at 218 K and 228 K.

Having derived an effective value of ΔH_{ads} for HNO_3 adsorption on cirrus cloud particles in the UT, HNO_3 coverages predicted by the Langmuir surface chemistry model (as a function of temperature) can be compared to the CRYSTAL-FACE observations (Fig. 11b). As in Fig. 11a, the isobaric lines are colored on the same scale as the observed coverages. The calculated coverages shown in Fig. 11b indicate that the model does not adequately describe the considerable variability in the observed coverages at a given temperature and $P(HNO_3)$. Nonetheless, when using the empirically derived ΔH_{ads} of -11.0 kcal·mol^{-1}, the Langmuir model is capable of predicting the observed coverages within a factor of 5 or better. The variability in the observed coverages, and the less than perfect agreement with the uptake models, can be explained, in part, if the adsorbed HNO_3 is not in equilibrium with HNO_3 in the gas phase. Previous field studies have also shown HNO_3 surface coverages to be highly variable throughout the temperature and $P(HNO_3)$ ranges observed [*Kondo et al.*, 2002, *Ziereis et al.*, 2003].

4.2. HNO_3 Partitioning in Cirrus Clouds

The fraction of total HNO_3 present on cirrus cloud particles was observed to increase with SAD during CRYSTAL-FACE (Fig. 13). The mean value of HNO_3 partitioned in the condensed phase at SADs greater than 200 μm^2·cm^{-3} was 16%. Up to 100% of the total HNO_3 was partitioned on ice particles during some cirrus cloud encounters, at SADs between 350 and $4.2\cdot10^4$ μm^2·cm^{-3} and temperatures between 201 K and 213 K. Measurements reported by *Ziereis et al.* [2003] in midlatitude cirrus clouds reveal a similar relationship between condensed-phase NO_y partitioning and SAD, although maximum reported values of condensed-phase NO_y partitioned in cirrus clouds did not exceed 50% of the total observed NO_y. Measurements of NO_y uptake in a mountain wave cirrus cloud reported by *Weinheimer et al.* [1998] indicate complete uptake of HNO_3, provided that the ambient HNO_3/NO_y ratio in the cloud was 0.1-0.2. Gas-phase HNO_3 was not measured in either of these previous studies, making an accurate assessment of the fraction of HNO_3 remaining in the gas phase after uptake difficult.

Krämer et al. [2003] have recently studied the partitioning of HNO_3 in Arctic cirrus clouds, and have modeled the role of HNO_3 uptake by interstitial HNO_3-H_2SO_4-H_2O ternary solution aerosols in partitioning. This study concluded that some fraction of the total HNO_3 in Arctic cirrus clouds must remain in the gas phase, with the remainder partitioned predominately in interstitial aerosols at temperatures less than 205 K when SADs are low, and on cirrus cloud particles at higher SADs. Measurements in subtropical cirrus clouds reported here, however, indicate that up to 100% of the total HNO_3 can be partitioned in cirrus ice particles both at low temperatures and low SADs. Furthermore, we see no evidence of significant uptake of HNO_3 in ternary solution aerosols outside of clouds in the subtropical UT during the flights considered in this study. There is evidence, however, of HNO_3 uptake by ternary solution aerosols in the near absence of cirrus ice particles on at least one other CRYSTAL-FACE flight (July 9, 2002) [*Weinheimer et al.*, 2002]. We also note that HNO_3 may be contained in a ternary solution on the surface of the cirrus ice particles.

4.3. HNO_3 and HNO_3/NO_y in the Cloud-Free Upper Troposphere and Lower Stratosphere

Measurements in the cloud-free subtropical UT during CRYSTAL-FACE indicate that the gas-phase HNO_3/NO_y ratio is highly variable, ranging from zero to approximately 0.5 (colored symbols in Fig. 14a). The HNO_3/NO_y ratio is generally higher and also variable in the subtropical lower stratosphere (LS), with values observed between 0.05 and 1 (black symbols in Fig. 14a). HNO_3 is expected to be the predominate NO_y species in the LS away from the tropopause region [*Neuman et al.*, 2001]. The lower HNO_3/NO_y ratios (< 0.3) observed in the UT are affected by low observed values of HNO_3, due to HNO_3 removal by uptake and sedimentation by cloud particles in cirrus processed air masses (yellow symbols in Fig. 14b), or from elevated levels of NO_y due to NO production from lightning strikes (purple symbols in Fig. 14b). Previously measured values of the HNO_3/NO_y ratio in the midlatitude UT over the continental United States were also highly variable and ranged from approximately 0.1 to 0.5 [*Neuman et al.*, 2001]. The large range and variability of HNO_3/NO_y ratios observed in the UT during CRYSTAL-FACE highlights the value in measuring gas-phase HNO_3 when assessing HNO_3 uptake on cirrus cloud particles, over deriving gas-phase HNO_3 from measured

NO_y and a constant assumed HNO_3/NO_y ratio.

A number of cirrus clouds observed in the subtropical UT during CRYSTAL-FACE had VMDs between 200 μm and 700 μm. Terminal fall velocities for cirrus ice particles in this size range are 1 $m{\cdot}s^{-1}$ to 10 $m{\cdot}s^{-1}$ (Fig. 9a) [*Meier and Hendricks*, 2002]. With 16% of the total HNO_3 in cirrus clouds adsorbed on ice particles, the gravitational redistribution of a significant fraction of the total HNO_3 in these clouds can therefore occur on a timescale of minutes to hours. Cirrus clouds with up to 100% of the total HNO_3 partitioned in the condensed phase have even greater potential to redistribute HNO_3 in the UT.

5. Conclusions and Implications

A number of cirrus cloud encounters in the UT by the NASA WB-57F during CRYSTAL-FACE were accompanied by the observation of condensed-phase HNO_3. Maximum levels of condensed-phase HNO_3 exceeded the gas-phase equivalent of 0.8 ppbv during some cirrus events. A mean HNO_3 surface coverage of $1.9{\cdot}10^{13}$ molecules$\cdot$cm^{-2} was observed on the flights of July 11, 13, 19 and 21, 2002, with maximum surface coverages reaching as high as $1.4{\cdot}10^{14}$ molecules$\cdot$cm^{-2} during a few cirrus cloud encounters. Molecular coverages predicted using a Langmuir surface chemistry model agree with the observed coverages to within a factor of 5 or better when using an empirically derived ΔH_{ads} of -11.0 kcal$\cdot$mol^{-1}. The mean percentage of total HNO_3 condensed on cirrus cloud particles was 16%, with up to 100% of the HNO_3 partitioned in the condensed phase in a number of cirrus clouds. The fraction of total HNO_3 in the condensed phase was found to increase strongly with SAD. Based on the large diameters of cloud particles containing HNO_3 observed during CRYSTAL-FACE, the redistribution of HNO_3 in the UT will be very effective in some cloud systems. The interpretation of future observations of HNO_3 uptake on cirrus particles will be improved by a knowledge of the individual history of the air parcels in which the cirrus clouds are formed [*Kärcher*, 2003] and laboratory studies of HNO_3 uptake at low gas-phase abundances ($P(HNO_3) < 2.0 \cdot 10^{-7}$ hPa) and low temperatures (195 K – 220 K).

Acknowledgements

The authors wish to thank the air and ground crews of the NASA WB-57F aircraft. Helpful discussions with J.P.D. Abbatt, E.R. Lovejoy and H. Ziereis are also appreciated. This work was partially supported by the National Aeronautics and Space Administration Upper Atmospheric Research Program and Radiation Science Program. Work done by MJM at the Jet Propulsion Laboratory, California Institute of Technology, was carried out under contract with the National Aeronautics and Space Administration.

References

Abbatt, J.P.D., Interaction of HNO_3 with water-ice surfaces at temperatures of the free troposphere, *Geophys. Res. Lett., 24*(12), 1479-1482, 1997.

Adamson, A.W. and A.P. Gast, *Physical Chemistry of Surfaces*, 6th Ed., John Wiley & Sons, New York, 1997.

Albritton, D.L., et al., Technical Summary of the Working Group I Report, in *Climate Change 2001: The Scientific Basis. Contribution of Working Group I to the Third Assessment Report of the Intergovernmental Panel on Climate Change*, edited by J.T. Houghton *et al.*, pp. 21-83, Cambridge University Press, Cambridge and New York, 2001.

Arora, O.P., et al., Uptake of nitric acid by sub-micron-sized ice particles, *Geophys. Res. Lett., 26*(24), 3621-3624, 1999.

Bartels-Rausch, T., et al., The adsorption enthalpy of nitrogen oxides on crystalline ice, *Atmos. Chem. Phys. 2*, 235-247, 2002.

Baumgardner, D., et al., The cloud, aerosol and precipitation spectrometer: a new instrument for cloud investigations, *Atmos. Res., 59-60*, 251-264, 2001.

Denning, R.F., S.L. Guidero, G.S. Parks, B.L. Gary, Instrument description of the Airborne Microwave Temperature Profiler, *J. Geophys. Res., 94,* 16,757-16,765, 1989.

Dominé, F. and E. Thibert, Mechanism of incorporation of trace gases in ice grown from the gas phase, *Geophys. Res. Lett., 23*(24), 3627-3630, 1996.

Gao, R.S., et al., Evidence that Ambient Nitric Acid Increases Relative Humidity in Low-Temperature Cirrus Clouds, In press. *Science*, 2003.

Gerber, H., Y. Takano, T.J. Garrett, and P.V. Hobbs, Nephelometer Measurements of the Asymmetry Parameter, Volume Extinction Coefficient, and Backscatter Ratio in Arctic Clouds, *J. Atmos. Sci. 57*, 3021-3034, 2000.

Hanson, D. and K. Mauersberger, Laboratory studies of the nitric acid trihydrate: implications for the south polar stratosphere, *Geophys. Res. Lett., 15*(8), 855-858, 1988.

Hanson, D.R. and A.R. Ravishankara, The reaction probabilities of $ClONO_2$ and N_2O_5 on polar stratospheric cloud materials, *J. Geophys. Res., 96*(3), 5081-5090, 1991.

Heymsfield, A.J. and G.M. McFarquhar, Mid-latitude and Tropical Cirrus: Microphysical Properties, in *Cirrus*, edited by D.K. Lynch, K. Sassen, D. O'C. Starr, and G. Stephens, pp. 78-101, Oxford University Press, Oxford, 2002.

Hudson, P.K., et al., Uptake of Nitric Acid on Ice at Tropospheric Temperatures: Implications for Cirrus Clouds, *J. Phys. Chem. A, 106*, 9874-9882, 2002.

Hynes, R.G., M.A. Fernandez, and R.A. Cox, Uptake of HNO_3 on water-ice and coadsorption of HNO_3 and HCl in the temperature range 210-235 K, *J. Geophys. Res., 107*(D24), 4797, doi:10.1029/2001JC001557, 2002.

Jaeglé, L., et al., Sources of HO_x and production of ozone in the upper troposphere over the United States, *Geophys. Res. Lett., 25*(10), 1709-1712, 1998.

Jin, Y., W.B. Rossow, D.P. Wylie, Comparison of the Climatologies of High-Level Clouds from HIRS and ISCCP, *J. Climate., 9*, 2850-2879, 1996.

Kärcher, B., Properties of subvisible cirrus clouds formed by homogeneous freezing, *Atmos. Chem. Phys., 2*, 161-170, 2002.

Kärcher, B., Simulating gas-aerosol-cirrus interactions: Process-oriented microphysical model and applications, *Atmos. Chem. Phys., 3*, 1645-1664, 2003.

Kondo, Y., et al., Uptake of reactive nitrogen on cirrus cloud particles in the upper troposphere and lowermost stratosphere, *Geophys. Res. Lett., 30*(4), 1154, doi:10.1029/2002GL016539, 2003.

Krämer, M., et al., Nitric acid partitioning in cirrus clouds: a synopsis based on field, laboratory and model studies, *Atmos. Chem. Phys. Discuss. 3*, 413-443, 2003.

Lacis, A.A., D.J. Wuebbles, and J.A. Logan, Radiative Forcing of Climate by Changes in the Vertical Distribution of Ozone, *J. Geophys. Res., 95*(D7), 9971-9982, 1990.

Laidler, K.J. and J.H. Meiser, *Physical Chemistry*, Benjamin Cummings, Menlo Park, 1982.

Lawrence, M.G. and P.J. Crutzen, The impact of cloud particle gravitational settling on soluble trace gas distributions, *Tellus, 50B*, 263-289, 1998.

Liao, X., W.B. Rossow, and D. Rind, Comparison between SAGE II and ISCCP high-level clouds: 1. Global and zonal mean cloud amounts, *J. Geophys. Res., 100*(D1), 1121-1135, 1995.

Liou, K.-N., Influence of Cirrus Clouds on Weather and Climate Processes: A Global Perspective, *Mon. Wea. Rev. 114*, 1167-1199, 1986.

Lynch, D.K., Cirrus History and Definition, in *Cirrus*, edited by D.K. Lynch, K. Sassen, D. O'C. Starr, and G. Stephens, pp. 3-10, Oxford University Press, Oxford, 2002.

Meier, A. and J. Hendricks, Model studies on the sensitivity of upper tropospheric chemistry to heterogeneous uptake of HNO_3 on cirrus ice particles, *J. Geophys. Res., 107*(D23), 4696, doi:10.1029/2001JD000735, 2002.

Meilinger, S.K., et al., HNO_3 Partitioning in Cirrus Clouds, *Geophys. Res. Lett. 26*(14), 2207-2210, 1999.

Neuman, J.A. et al., Study of Inlet Materials for Sampling Atmospheric Nitric Acid, *33,* 1133-1136, 1999.

Neuman, J.A. et al., A fast-response chemical ionization mass spectrometer for *in situ* measurements of HNO_3 in the upper troposphere and lower stratosphere, *Rev. Sci. Instrum., 71*(10), 3886-3892, 2000.

Neuman, J.A., et al., In situ measurements of HNO_3, NO_y, NO, and O_3 in the lower stratosphere and upper troposphere, *Atmos. Environ., 35*, 5789-5797, 2001.

Northway, M.J., et al., An analysis of large HNO_3-containing particles sampled in the Arctic stratosphere during the winter of 1999/2000, *J. Geophys. Res., 107*(D20), 8298, doi:10.1029/2001JD001079, 2002.

Sassen, K., Cirrus Clouds: A Modern Perspective, in *Cirrus*, edited by D.K. Lynch, K. Sassen, D. O'C. Starr, and G. Stephens, pp. 11-40, Oxford University Press, Oxford, 2002.

Scott, S.G., T.P. Bui, K.R. Chan, and S.W. Bowen, The meteorological measurement system on the NASA ER-2 aircraft, *J. Atmos. Oceanic Technol., 7*, 525-540, 1990.

Sommerfeld, R.A., C.A. Knight and S.K. Laird, Diffusion of HNO_3 in ice, *Geophys. Res. Lett., 25*(6), 935-938, 1998.

Tabazadeh, A., O.B. Toon, E.J. Jensen, A surface chemistry model for nonreactive trace gas adsorption on ice: Implications for nitric acid scavenging by cirrus, *Geophys. Res. Lett., 26*(14), 2211-2214, 1999.

Vincent, J.H., et al., On the aspiration characteristics of large-diameter thin-walled aerosol sampling probes at yaw orientations with respect to the wind, *J. Aerosol Sci. 17*(2), 211-224, 1986.

Wang, P.-H., et al., A 6-year climatology of cloud occurrence frequency from Stratospheric Aerosol and Gas Experiment II observations (1985-1990), *J. Geophys. Res., 101*(D23), 29407-29,429, 1996.

Weinheimer, A.J. et al., Manuscript in preparation. 2004.

Weinheimer, A.J., et al., Uptake of NO_y on wave-cloud ice particles, *Gephys. Res. Lett., 25*(10), 1725-1728, 1998.

Weinstock, E.M., et al., New fast-response photofragment fluorescence hygrometer for use on the NASA ER-2 and the Perseus remotely piloted aircraft, *Rev. Sci. Instrum., 65*(11), 3544-3554, 1994.

Weinstock, E.M. et al., Manuscript in preparation. 2004.

Wylie, D.P., and Menzel, W.P., Eight Years of High Cloud Statistics Using HIRS, *J. Climate, 12,* 170-184, 1999.

Ziereis, H. et al., Uptake of reactive nitrogen on cirrus cloud particles during INCA, Submitted to *Geophys. Res. Lett.*

Zondlo, M.A., S.B. Barone, and M.A. Tolbert, Uptake of HNO_3 on ice under upper tropospheric conditions, *Geophys. Res. Lett., 24*(11), 1391-1394, 1997.

Figure Captions

Figure 1. Schematic diagram of the NOAA CIMS inlet pylon. Labeled components are as follows: (a) front channel inlet, (b) bottom channel inlet, (c) zero gas addition, (d) calibration gas addition, (e) reagent gas carrier addition, (f) reagent gas addition, (g) HNO_3 permeation cell (calibration standard), (h) flow control valve motor, (i) flow control valve body, (j) flow tube, (k) ion source, (l) flow straightener. For clarity, complete components are shown only for the front channel. Inlet lines are constructed of Teflon™ tubing (6.4 mm outside diameter, 4.0 mm inside diameter), heated to temperatures of 40° C (bottom channel inlet) and 48° C (front channel inlet) to avoid wall losses. The higher temperature of the front inlet ensures that ice particles entering the inlet evaporate upon impaction with the tubing wall. The operating principles of the NOAA CIMS instrument have been described in detail by *Neuman et al.* [2000].

Figure 2. Time series measurements of the HNO_3 mixing ratio observed from the front and bottom CIMS channels ($HNO_3|_{front}$ and $HNO_3|_{gas}$, respectively,) on the flight of July 11, 2002. Note that values of $HNO_3|_{front}$ do not include a correction for particle oversampling in the front channel inlet. Discontinuities in the time series result from CIMS instrument calibrations and other housekeeping procedures. Also shown are SAD, IWC, water vapor, relative humidity (with respect to ice), and ambient temperature and pressure. All data are represented as 10-s averages. Minor divisions on the horizontal scale represent 15 minutes (or approximately 150 km) of flight.

Figure 3. Same as Fig. 2, for the flight on July 13, 2002. Purple bars in panel (b) represent 3 flight segments in which cirrus clouds formed in the contrail of the WB-57F were observed. The inset in panel (a) shows 1-s averages of $HNO_3|_{front}$ and $HNO_3|_{gas}$ during the first contrail intercept. The purple bar in the inset represents the same time period as the first purple bar in panel (b). The vertical scale on the inset panel is 0 to 1 ppbv. Measurements of $HNO_3|_{front}$ and $HNO_3|_{gas}$ are incomplete during the second and third contrail intercepts due to instrument housekeeping procedures.

Figure 4. Same as Fig. 2, for the flight on July 19, 2002. Purple bars in panel (b) represent 2 flight segments in which cirrus clouds formed in the contrail of the WB-57F were observed. The insets in panel (a) shows 1-s averages of $HNO_3|_{front}$ and $HNO_3|_{gas}$ during the two contrail intercepts. The purple bars in the first and second insets represent the same time periods as the first and second purple bars in panel (b). The vertical scale on the inset panels is 0 to 0.5 ppbv.

Figure 5. Same as Fig. 2, for the flight on July 21, 2002.

Figure 6. ($HNO_3|_{front}$ - $HNO_3|_{gas}$) vs. SAD for the flights of July 11, 13, 19 and 21, 2002. Values of ($HNO_3|_{front}$ -$HNO_3|_{gas}$) are proportional, but not equal to condensed-phase HNO_3 ($HNO_3|_{con}$) because they do not include a correction for particle

oversampling in the front channel inlet. Red circles represent 10-s averages and black squares represent mean values of the 10-s data grouped into deciles. Vertical bars represent the standard deviation about the mean value in each decile, and horizontal bars indicate the upper and lower boundaries of each decile. Note that the vertical axis is shown with a logarithmic scale at values greater than 2.5. The dashed vertical line at the SAD of 200 $\mu m^2 \cdot cm^{-3}$ represents the lower limit chosen here to represent measurements made in cirrus clouds.

Figure 7. Calculation of $HNO_3|_{con}$ for a cirrus cloud encounter by the NASA WB-57F on July 13, 2002, showing $HNO_3|_{front}$ and $HNO_3|_{gas}$ (panel a), *EF* (panel b), $HNO_3|_{con}$ (panel c), SAD (panel d) and IWC (panel e). All data are shown as 10-s averages. The horizontal axis spans approximately 16 minutes and 180 km of flight.

Figure 8. Comparison of CIN- and CAPS-derived SAD measured during the flights of July 11, 13, 19 and 21, 2002. Data at SADs less than 3 $\mu m^2 \cdot cm^{-3}$ are expanded in the inset. All data are shown as 10-s averages. Lines represent a least-squares fit to the data for each flight date. The slope of the linear fit (constrained through the origin) is shown for each flight date in the figure legend.

Figure 9. Panel (a). Volume-weighted mean diameter of cirrus cloud particles vs. SAD measured during the flights on July 11, 13, 19 and 21, 2002. Only data at SADs greater than 200 $\mu m^2 \cdot cm^{-3}$ are shown. Data are colored according to ambient temperature. The black line represents the terminal fall velocity for ice particles in the upper troposphere, calculated according to *Meier and Hendricks* [2002]. Panel (b). IWC (represented as a gas-phase equivalent volume mixing ratio) vs. SAD. At 130 hPa and 200 K, an IWC of 100 ppmv is equivalent to an ice water concentration of 14 $mg \cdot m^{-3}$. Other details same as panel (a).

Figure 10. HNO_3 coverage vs. temperature for measurements made in cirrus clouds at SADs greater than 200 $\mu m^2 \cdot cm^{-3}$ on July 11, 13, 19 and 21, 2002. Symbols are colored according to $P(HNO_3)$. Triangles at temperatures less than 200 K indicate measurements made under conditions in which NAT is stable. Mean values of HNO_3 coverage are plotted at the mean of 5 K temperature bins from 195 K to 220 K (black squares). Error bars represent the standard deviation in each temperature bin. Negative values of HNO_3 coverage are included in the calculation of the mean values. The dashed line at $1.9 \cdot 10^{13}$ molecules$\cdot cm^{-2}$ represents the mean HNO_3 coverage observed during CRYSTAL-FACE. A complete HNO_3 monolayer is formed when the coverage reaches $1.0 \cdot 10^{15}$ molecules$\cdot cm^{-2}$.

Figure 11. HNO_3 coverage vs. temperature for measurements made in cirrus clouds at SADs greater than 200 $\mu m^2 \cdot cm^{-3}$ on July 11, 13, 19 and 21, 2002. Symbols are colored according to $P(HNO_3)$. Triangles at temperatures less than 200 K indicate measurements made under conditions in which NAT is stable. Data are represented as 10-s averages.

Panel (a). Lines are isobars representing HNO_3 coverages calculated by the FHH HNO_3 uptake model [*Hudson et al.*, 2002] and are colored according to the same temperature scale as the observed coverages (see legend). Panel (b). Same as panel (a), except the isobars represent HNO_3 coverages calculated by the Langmuir surface chemistry model.

Figure 12. Fractional HNO_3 surface coverage (θ) vs. $P(HNO_3)$ measured during the flights of July 11, 13, 19 and 21, 2002. Colored lines are isotherms fitted according to equations (2) and (3) (see text) with values of ΔH_{ads} shown in the legend and the median observed temperature of 208 K. All data are represented as 10-s averages for measurements made at SADs greater than 200 $\mu m^2 \cdot cm^{-3}$.

Figure 13. Fraction of total HNO_3 in the condensed phase vs. SAD measured during the flights of July 11, 13, 19 and 21, 2002. Data are represented as 10-s averages for measurements made at SADs greater than 200 $\mu m^2 \cdot cm^{-3}$ and are colored according to temperature. Black squares represent mean values of the 10-s data grouped into quintiles. Vertical bars represent the standard deviation about the mean value in each quintile and horizontal bars represent the upper and lower boundaries of each quintile. Values of condensed-phase partitioning greater than 100% occur when zero or near-zero $HNO_3|_{gas}$ abundances are measured as negative values. The dashed line at 16% represents the mean value of HNO_3 partitioned in the condensed phase during CRYSTAL-FACE.

Figure 14. Panel (a). Vertical profile of the gas-phase HNO_3/NO_y ratio observed in cloud free air (SADs less than 20 $\mu m^2 \cdot cm^{-3}$) during the flights of July 11, 13, 19 and 21, 2002. Tropospheric measurements (according to the Microwave Temperature Profiler) are colored according to measured NO. Stratospheric measurements are shown in black. Panel (b). Vertical profile of $HNO_3|_{gas}$. Other details same as panel (a).

Table 1. Measurement details.

Measurement	Institution	Precision[a]	Accuracy	Reference.
HNO_3	NOAA Aeronomy Lab	30 pptv, 10 pptv[b]	±20%	*Neuman et al.*, 2002
SAD - CAPS	Univ. Nacional Autonoma de Mexico	-	±50%	*Baumgardner et al.*, 2002
SAD - CIN	University of Utah	-	±15%	*Gerber et al.*, 2000
IWC	Harvard University	0.7 ppmv	±17%	*Weinstock et al.*, 2004
Water Vapor	Harvard University	0.5 ppmv	±5%	*Weinstock et al.*, 1994
NO	NCAR	5 pptv	±6%	*Weinheimer et al.*, 2004
NO_y	NCAR	8 pptv	±12%	*Weinheimer et al.*, 2004
Temperature	NASA Ames	0.01 K	±0.3 K	*Scott et al.*, 1990
Pressure	NASA Ames	0.1 hPa	±0.3 hPa	*Scott et al.*, 1990
True Air Speed	NASA Ames	$0.1\ m \cdot s^{-1}$	$\pm 1\ m \cdot s^{-1}$	*Scott et al.*, 1990

[a] Precision values are reported for 10-s averages

[b] 10 pptv is the precision for condensed-phase HNO_3.

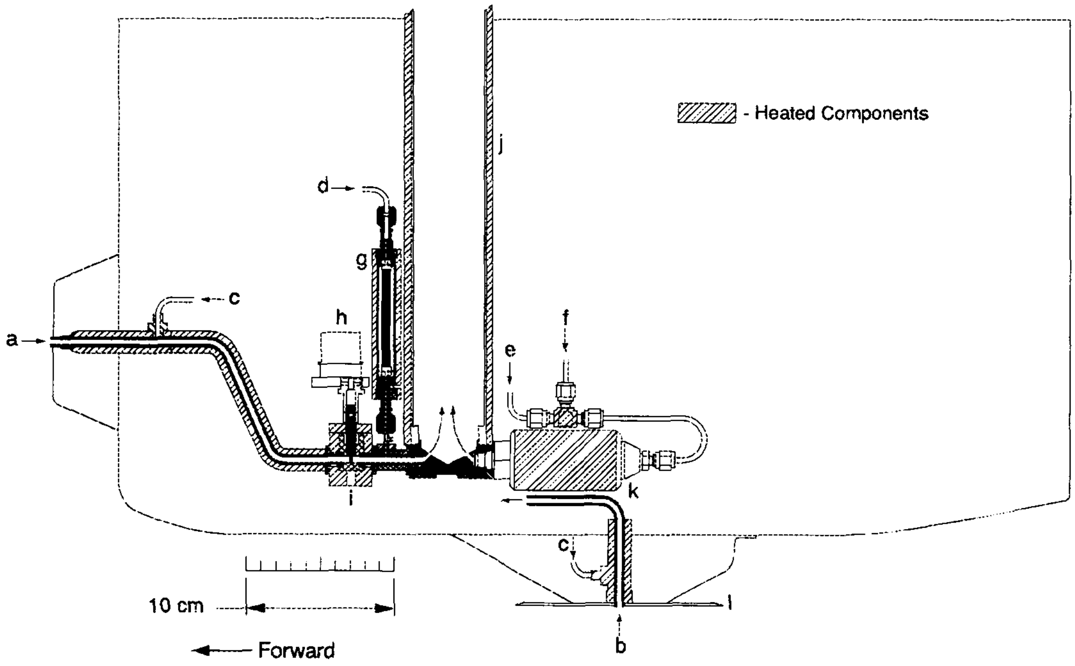

Fig. 1 Popp et al.

Figure 1. Schematic diagram of the NOAA CIMS inlet pylon. Labeled components are as follows: (a) front channel inlet, (b) bottom channel inlet, (c) zero gas addition, (d) calibration gas addition, (e) reagent gas carrier addition, (f) reagent gas addition, (g) HNO_3 permeation cell (calibration standard), (h) flow control valve motor, (i) flow control valve body, (j) flow tube, (k) ion source, (l) flow straightener. For clarity, complete components are shown only for the front channel. Inlet lines are constructed of Teflon$^{\text{TM}}$ tubing (6.4 mm outside diameter, 4.0 mm inside diameter), heated to temperatures of 40° C (bottom channel inlet) and 48° C (front channel inlet) to avoid wall losses. The higher temperature of the front inlet ensures that ice particles entering the inlet evaporate upon impaction with the tubing wall. The operating principles of the NOAA CIMS instrument have been described in detail by *Neuman et al.* [2000].

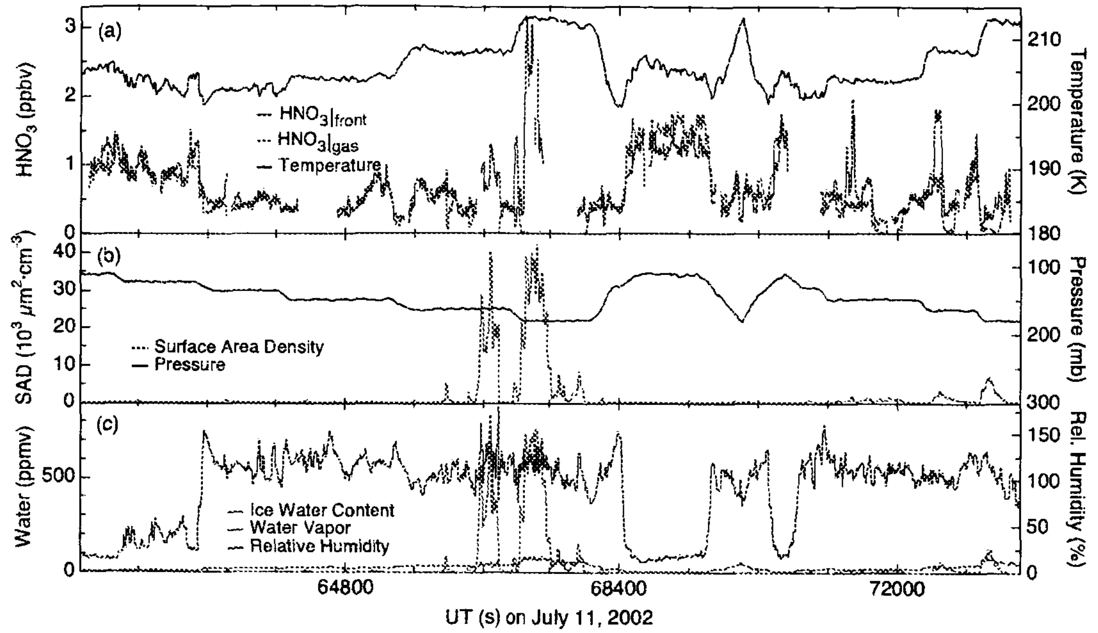

Fig. 2 Popp et al.

Figure 2. Time series measurements of the HNO_3 mixing ratio observed from the front and bottom CIMS channels ($HNO_3|_{front}$ and $HNO_3|_{gas}$, respectively,) on the flight of July 11, 2002. Note that values of $HNO_3|_{front}$ do not include a correction for particle oversampling in the front channel inlet. Discontinuities in the time series result from CIMS instrument calibrations and other housekeeping procedures. Also shown are SAD, IWC, water vapor, relative humidity (with respect to ice), and ambient temperature and pressure. All data are represented as 10-s averages. Minor divisions on the horizontal scale represent 15 minutes (or approximately 150 km) of flight.

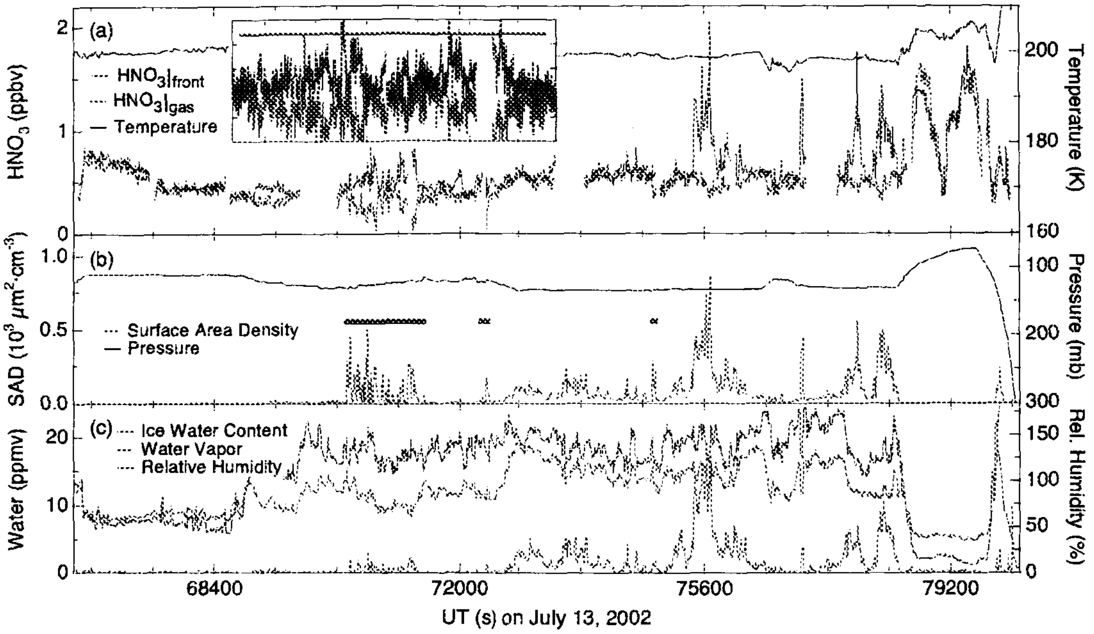

Fig. 3 Popp et al.

Figure 3. Same as Fig. 2, for the flight on July 13, 2002. Purple bars in panel (b) represent 3 flight segments in which cirrus clouds formed in the contrail of the WB-57F were observed. The inset in panel (a) shows 1-s averages of $HNO3|_{front}$ and $HNO3|_{gas}$ during the first contrail intercept. The purple bar in the inset represents the same time period as the first purple bar in panel (b). The vertical scale on the inset panel is 0 to 1 ppbv. Measurements of $HNO3|_{front}$ and $HNO3|_{gas}$ are incomplete during the second and third contrail intercepts due to instrument housekeeping procedures.

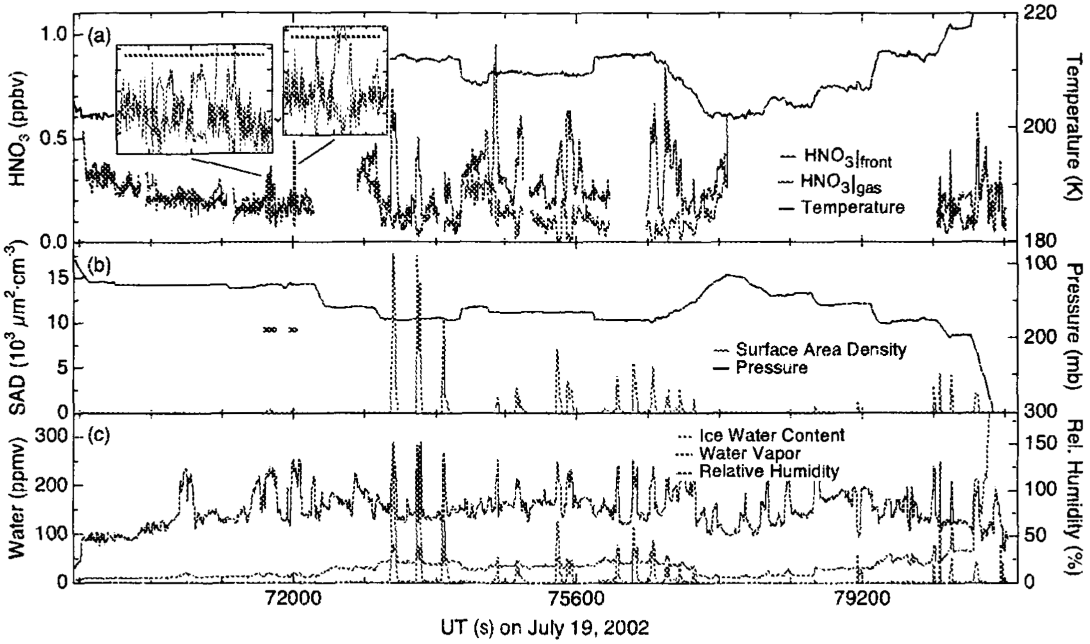

Fig. 4 Popp et al.

Figure 4. Same as Fig. 2, for the flight on July 19, 2002. Purple bars in panel (b) represent 2 flight segments in which cirrus clouds formed in the contrail of the WB-57F were observed. The insets in panel (a) shows 1-s averages of $HNO3l_{front}$ and $HNO3l_{gas}$ during the two contrail intercepts. The purple bars in the first and second insets represent the same time periods as the first and second purple bars in panel (b). The vertical scale on the inset panels is 0 to 0.5 ppbv.

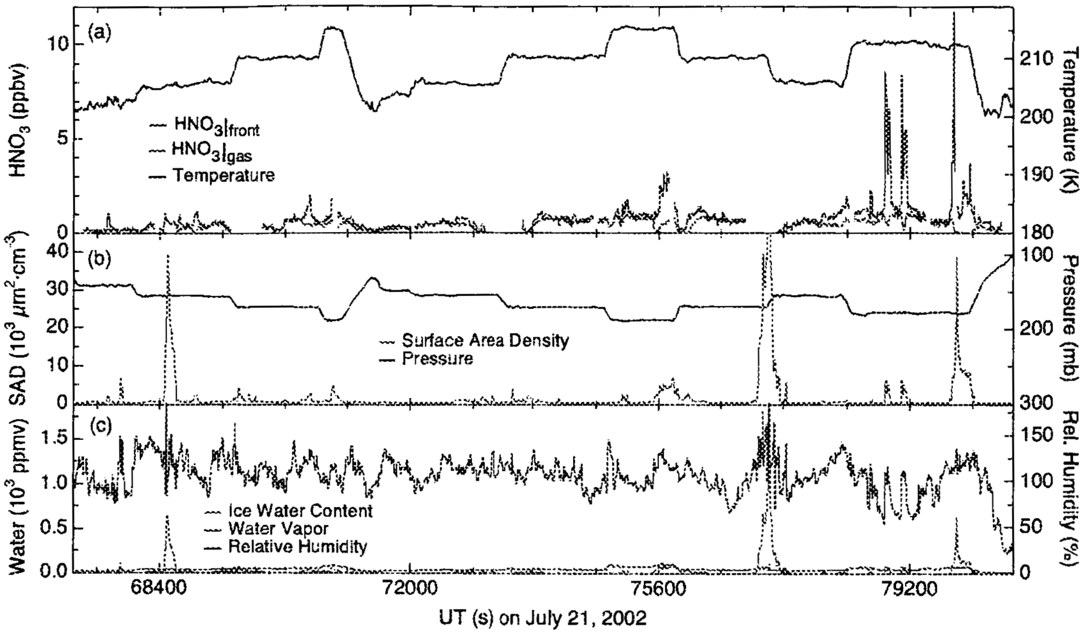

Fig. 5 Popp et al.

Figure 5. Same as Fig. 2, for the flight on July 21, 2002.

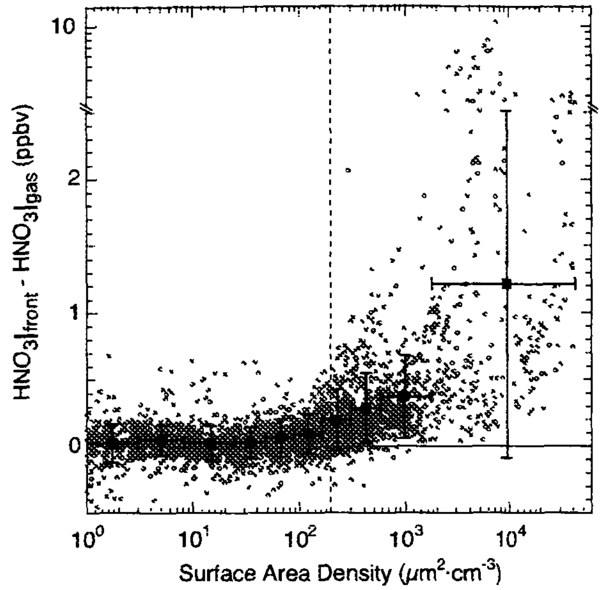

Fig. 6 Popp et al.

Figure 6. ($HNO_3|_{front}$ - $HNO_3|_{gas}$) vs. SAD for the flights of July 11, 13, 19 and 21, 2002. Values of ($HNO_3|_{front}$ -$HNO_3|_{gas}$) are proportional, but not equal to condensed-phase HNO_3 ($HNO_3|_{con}$) because they do not include a correction for particle oversampling in the front channel inlet. Red circles represent 10-s averages and black squares represent mean values of the 10-s data grouped into deciles. Vertical bars represent the standard deviation about the mean value in each decile, and horizontal bars indicate the upper and lower boundaries of each decile. Note that the vertical axis is shown with a logarithmic scale at values greater than 2.5. The dashed vertical line at the SAD of 200 $\mu m^2 \cdot cm^{-3}$ represents the lower limit chosen here to represent measurements made in cirrus clouds.

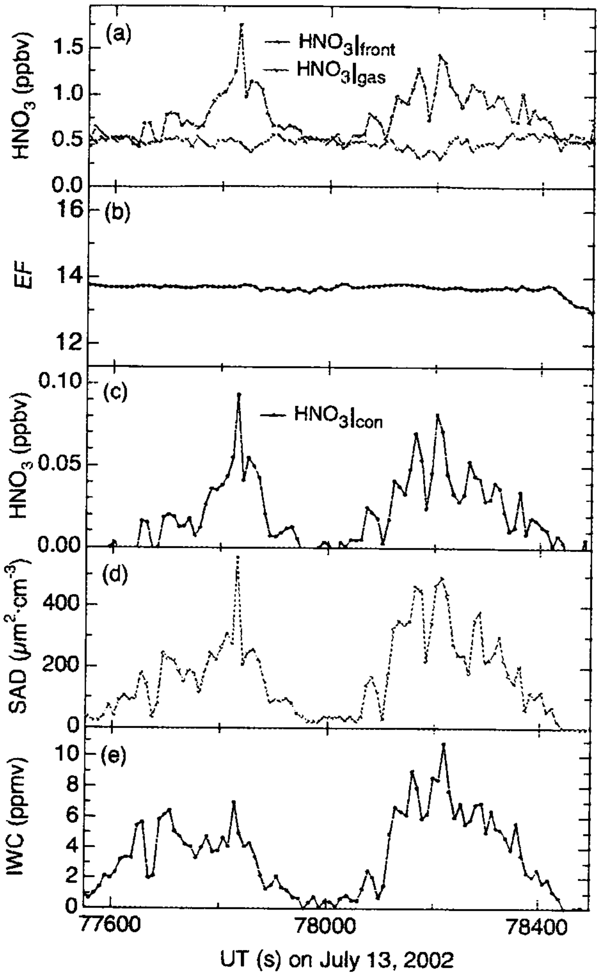

Fig. 7 Popp et al.

Figure 7. Calculation of $HNO3|_{con}$ for a cirrus cloud encounter by the NASA WB-57F on July 13, 2002, showing $HNO3|_{front}$ and $HNO3|_{gas}$ (panel a), *EF* (panel b), $HNO3|_{con}$ (panel c), SAD (panel d) and IWC (panel e). All data are shown as 10-s averages. The horizontal axis spans approximately 16 minutes and 180 km of flight.

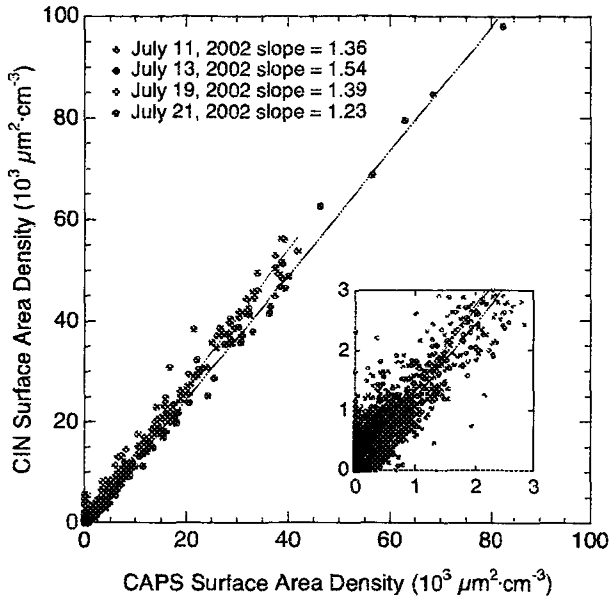

Fig. 8 Popp et al.

Figure 8. Comparison of CIN- and CAPS-derived SAD measured during the flights of July 11, 13, 19 and 21, 2002. Data at SADs less than 3 μm^2·cm^{-3} are expanded in the inset. All data are shown as 10-s averages. Lines represent a least-squares fit to the data for each flight date. The slope of the linear fit (constrained through the origin) is shown for each flight date in the figure legend.

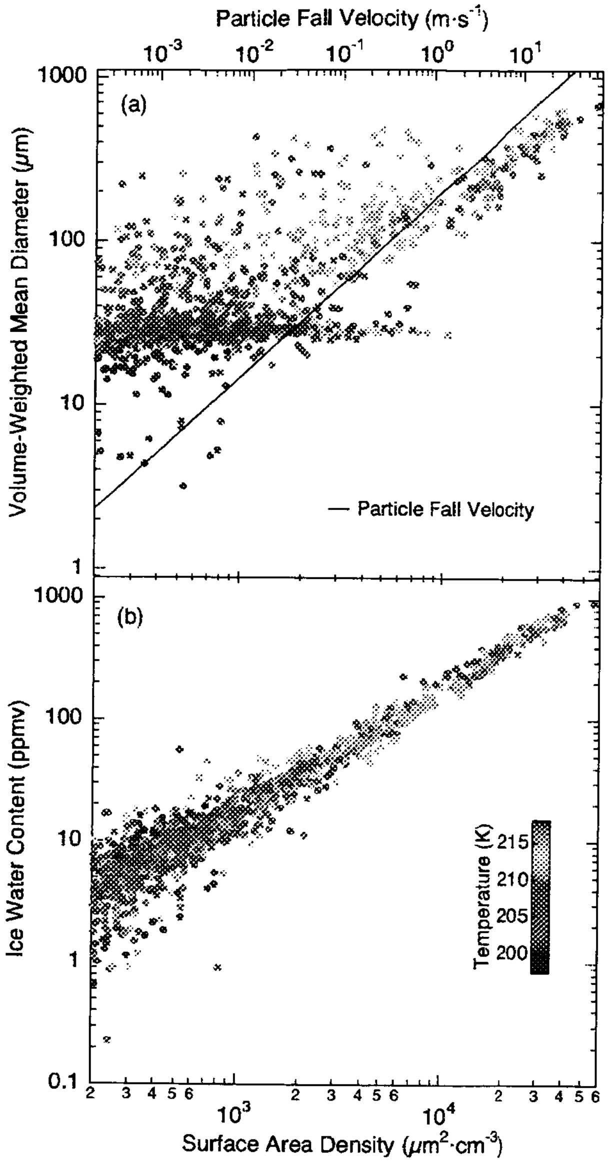

Fig. 9 Popp et al.

Figure 9. Panel (a). Volume-weighted mean diameter of cirrus cloud particles vs. SAD measured during the flights on July 11, 13, 19 and 21, 2002. Only data at SADs greater than 200 $\mu m^2 \cdot cm^{-3}$ are shown. Data are colored according to ambient temperature. The black line represents the terminal fall velocity for ice particles in the upper troposphere, calculated according to *Meier and Hendricks* [2002]. Panel (b). IWC (represented as a gas-phase equivalent volume mixing ratio) vs. SAD. At 130 hPa and 200 K, an IWC of 100 ppmv is equivalent to an ice water concentration of 14 mg·m^{-3}. Other details same as panel (a).

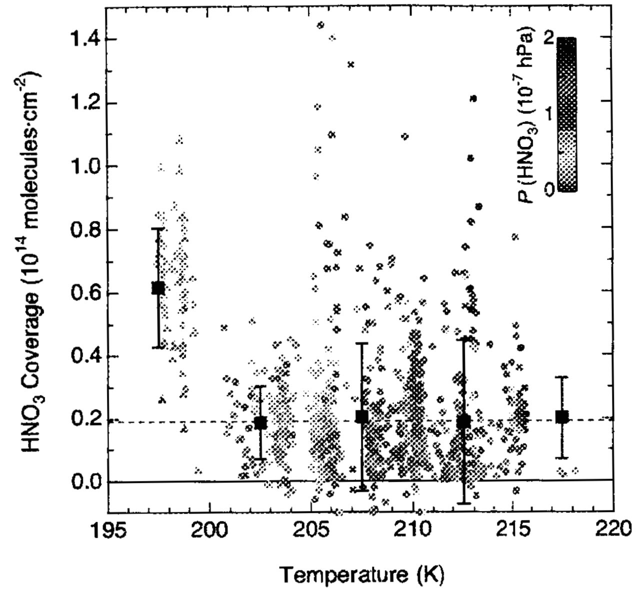

Fig. 10 Popp et al.

Figure 10. HNO_3 coverage vs. temperature for measurements made in cirrus clouds at SADs greater than 200 $\mu m^2 \cdot cm^{-3}$ on July 11, 13, 19 and 21, 2002. Symbols are colored according to $P(HNO_3)$. Triangles at temperatures less than 200 K indicate measurements made under conditions in which NAT is stable. Mean values of HNO_3 coverage are plotted at the mean of 5 K temperature bins from 195 K to 220 K (black squares). Error bars represent the standard deviation in each temperature bin. Negative values of HNO_3 coverage are included in the calculation of the mean values. The dashed line at $1.9 \cdot 10^{13}$ molecules·cm^{-2} represents the mean HNO_3 coverage observed during CRYSTAL-FACE. A complete HNO_3 monolayer is formed when the coverage reaches $1.0 \cdot 10^{15}$ molecules·cm^{-2}.

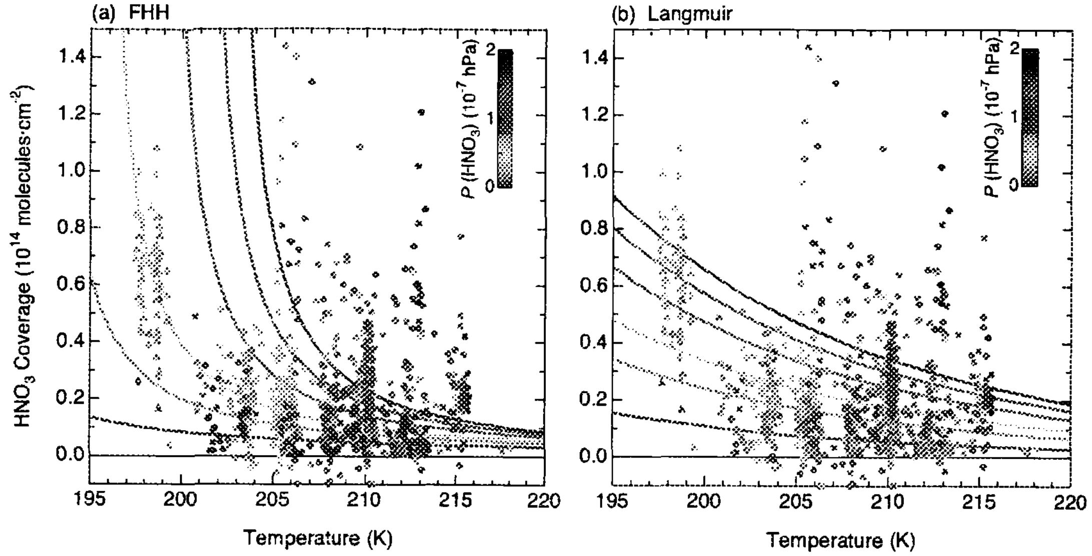

Fig. 11 Popp et al.

Figure 11. HNO_3 coverage vs. temperature for measurements made in cirrus clouds at SADs greater than 200 $\mu m^2 \cdot cm^{-3}$ on July 11, 13, 19 and 21, 2002. Symbols are colored according to $P(HNO_3)$. Triangles at temperatures less than 200 K indicate measurements made under conditions in which NAT is stable. Data are represented as 10-s averages. Panel (a). Lines are isobars representing HNO_3 coverages calculated by the FHH HNO_3 uptake model [*Hudson et al.*, 2002] and are colored according to the same temperature scale as the observed coverages (see legend). Panel (b). Same as panel (a), except the isobars represent HNO_3 coverages calculated by the Langmuir surface chemistry model.

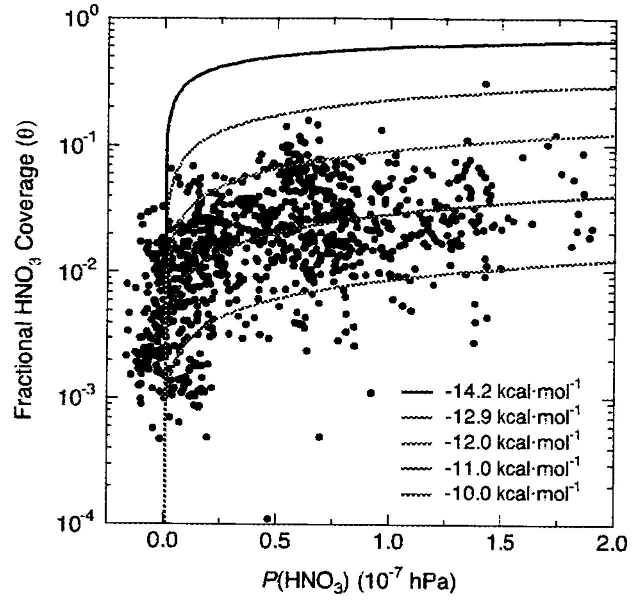

Fig. 12 Popp et al.

Figure 12. Fractional HNO_3 surface coverage (θ) vs. $P(HNO_3)$ measured during the flights of July 11, 13, 19 and 21, 2002. Colored lines are isotherms fitted according to equations (2) and (3) (see text) with values of ΔH_{ads} shown in the legend and the median observed temperature of 208 K. All data are represented as 10-s averages for measurements made at SADs greater than 200 $\mu m^2 \cdot cm^{-3}$.

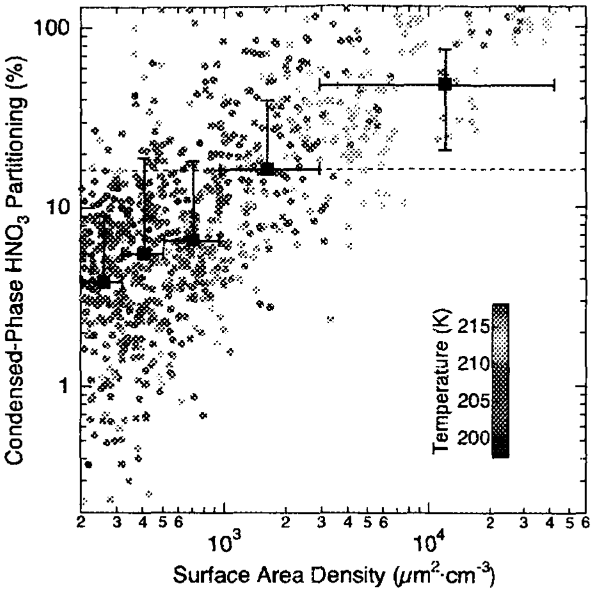

Fig. 13 Popp et al.

Figure 13. Fraction of total HNO3 in the condensed phase vs. SAD measured during the flights of July 11, 13, 19 and 21, 2002. Data are represented as 10-s averages for measurements made at SADs greater than 200 $\mu m^2 \cdot cm^{-3}$ and are colored according to temperature. Black squares represent mean values of the 10-s data grouped into quintiles. Vertical bars represent the standard deviation about the mean value in each quintile and horizontal bars represent the upper and lower boundaries of each quintile. Values of condensed-phase partitioning greater than 100% occur when zero or near-zero $HNO3|_{gas}$ abundances are measured as negative values. The dashed line at 16% represents the mean value of HNO3 partitioned in the condensed phase during CRYSTAL-FACE.

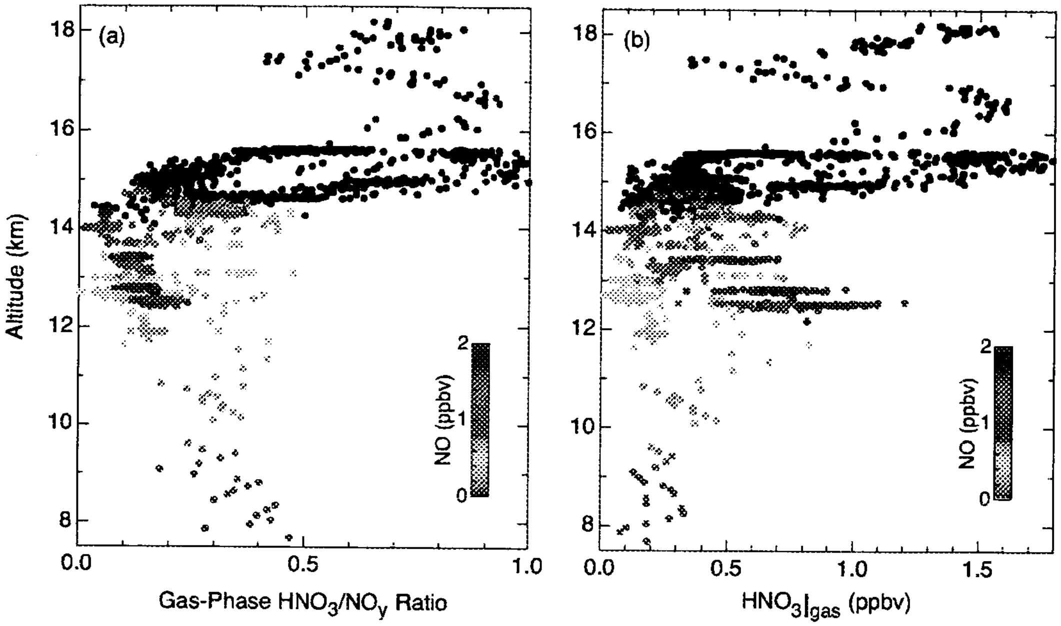

Fig. 14 Popp et al.

Figure 14. Panel (a). Vertical profile of the gas-phase HNO_3/NO_y ratio observed in cloud free air (SADs less than 20 $\mu m^2 \cdot cm^{-3}$) during the flights of July 11, 13, 19 and 21, 2002. Tropospheric measurements (according to the Microwave Temperature Profiler) are colored according to measured NO. Stratospheric measurements are shown in black. Panel (b). Vertical profile of $HNO_3|_{gas}$. Other details same as panel (a).